

**Highly sensitive band structure of the Stoner-enhanced Pauli paramagnet SrCo<sub>2</sub>P<sub>2</sub>**K. Götze<sup>1,2</sup>, I. Kraft,<sup>3</sup> J. Klotz,<sup>1,4</sup> T. Förster,<sup>1</sup> M. Uhlarz,<sup>1</sup> V. Lorenz,<sup>3</sup> C. Bergmann,<sup>3</sup> Y. Prots,<sup>3</sup> J. A. N. Bruin,<sup>5</sup> A. McCollam,<sup>5</sup> I. Sheikin,<sup>6</sup> J. Wosnitza,<sup>1,4</sup> C. Geibel<sup>3</sup> and H. Rosner<sup>3</sup><sup>1</sup>*Hochfeld-Magnetlabor Dresden (HLD-EMFL), Würzburg-Dresden Cluster of Excellence ct.qmat, Helmholtz-Zentrum Dresden-Rossendorf, 01328 Dresden, Germany*<sup>2</sup>*Department of Physics, University of Warwick, Coventry CV4 7AL, United Kingdom*<sup>3</sup>*Max Planck Institute for Chemical Physics of Solids, 01187 Dresden, Germany*<sup>4</sup>*Institut für Festkörper- und Materialphysik, Technische Universität Dresden, 01062 Dresden, Germany*<sup>5</sup>*High Field Magnet Laboratory (HFML-EMFL), Radboud University, 6525 ED Nijmegen, The Netherlands*<sup>6</sup>*Laboratoire National des Champs Magnétiques Intenses (LNCMI-EMFL), CNRS, UGA, 38042 Grenoble, France*

(Received 20 April 2021; accepted 13 August 2021; published 25 August 2021)

The compound SrCo<sub>2</sub>P<sub>2</sub> is a Pauli paramagnet very close to ferromagnetic order. To study its electronic structure in close vicinity to the Fermi level, we report measurements of the de Haas–van Alphen effect in magnetic fields up to 35 T in combination with density-functional-theory band-structure calculations in different approximations. The resulting electronic band structure not only depends significantly on the choice of the functional, but also crucially on the exact values of the structural parameters that have been determined at low temperatures by synchrotron x-ray diffraction. We find the best correspondence between the measured and the calculated de Haas–van Alphen frequencies for the general gradient approximation functional and the structural parameters that were determined at 10 K. Although SrCo<sub>2</sub>P<sub>2</sub> crystallizes in the uncollapsed tetragonal structure with a large P-P distance between the Co<sub>2</sub>P<sub>2</sub> layers, we observe a rather three-dimensional Fermi-surface topology. We obtain a mass-enhancement factor of about 2 deduced from the ratio between experimental and calculated quasiparticle masses. The temperature dependence of the structural parameters leads to a significant reduction of the electronic density of states at the Fermi level and in comparison with the measured Sommerfeld coefficient to an overall mass renormalization in line with our experiment.

DOI: [10.1103/PhysRevB.104.085148](https://doi.org/10.1103/PhysRevB.104.085148)**I. INTRODUCTION**

The metallic compounds that crystallize in the ThCr<sub>2</sub>Si<sub>2</sub> structure, such as some iron-based superconductors, exhibit a large variety of magnetic and electronic properties including quantum criticality and heavy-fermion behavior [1,2]. They generally have the form AT<sub>2</sub>X<sub>2</sub>, with A being a rare-earth, alkali, or alkaline-earth metal, T being a transition metal, and X is an element from the carbon or nitrogen group. Two important parameters that determine the magnetic properties and the occurrence of superconductivity in these systems are the distance  $d_{X-X}$  and the X position within the T<sub>2</sub>X<sub>2</sub> layers.

The bonding between the T<sub>2</sub>X<sub>2</sub> layers in these systems varies with the distance  $d_{X-X}$  from unbound for large  $d_{X-X}$  to a fully developed X-X bonding for small  $d_{X-X}$  [3]. The former case, the uncollapsed tetragonal (ucT) state, usually has a two-dimensional electronic structure, whereas the strong X-X bonding in the collapsed tetragonal (cT) structure pulls the T<sub>2</sub>X<sub>2</sub> layers together leading to a more three-dimensional Fermi surface (FS) [4–6]. A transition between the two states, induced by pressure or chemical substitution [7,8], can change the physical properties strongly. CaFe<sub>2</sub>As<sub>2</sub>, for example, becomes superconducting after a structural phase transition from ucT to cT under a pressure of 0.35 GPa [9,10] implying

that the strength of the bonding in AT<sub>2</sub>X<sub>2</sub> materials plays an important role in the emergence of superconductivity [11].

The pnictide position, expressed in the distance  $z_X$  and the T-X bonding angle, varies on a smaller scale than  $d_{X-X}$ , but it also has a decisive influence on the electronic properties of the material. For example, in the superconducting iron arsenides a small variation of the bonding angle or the height of As to the Fe planes can alter the superconducting critical temperature substantially [12,13], which reaches its highest value in NdFeAsO<sub>1-y</sub> for a regular tetrahedron of the FeAs<sub>4</sub> pyramids [14].

The bond angle in the transition-metal-pnictide layers might also play an important role in the occurrence of magnetic order. For example, the arsenides where this angle is close to the ideal value of 109.47°, order magnetically whereas the pnictides that have a bond angle that differs from this optimum do not order [6].

SrCo<sub>2</sub>P<sub>2</sub> belongs to the family of AT<sub>2</sub>X<sub>2</sub> compounds and has a ucT structure with a long-distance  $d_{P-P}$  of 3.425 Å at 10 K. The unit cell is shown in the inset of Fig. 1(a). SrCo<sub>2</sub>P<sub>2</sub> does not become superconducting and shows a Stoner-enhanced Pauli paramagnetism being nearly ferromagnetic [8]. In 2010, Jia and Cava reported that ferromagnetism in SrCo<sub>2</sub>P<sub>2</sub> can be induced upon substitution of Sr by La, placing the compound close to a quantum critical point [15].

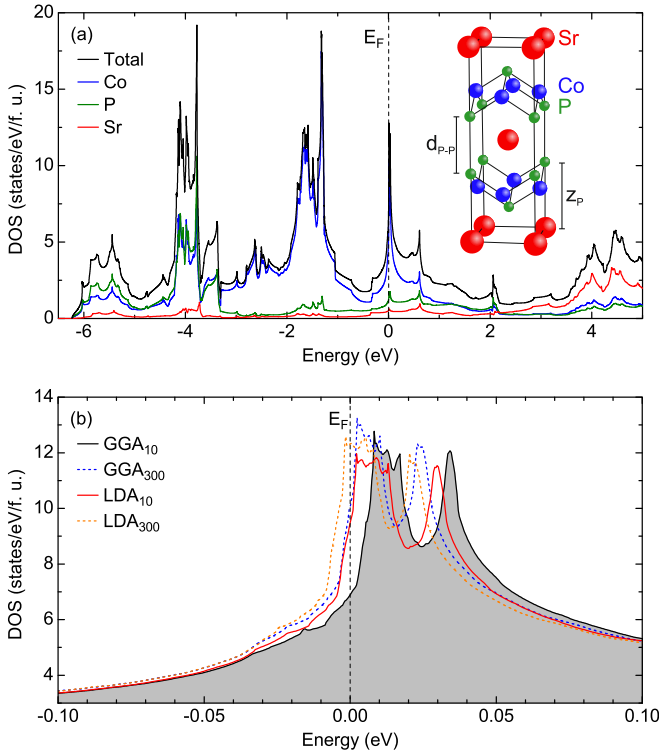


FIG. 1. (a) Total and atomically resolved partial density of states for  $\text{SrCo}_2\text{P}_2$  calculated by use of the FPLO code with the GGA functional and lattice parameters at 10 K. The inset shows the crystal structure of  $\text{SrCo}_2\text{P}_2$  with the distance  $d_{p,p}$  of 3.425 Å. (b) Zoom of the total DOS around  $E_F$  calculated using the LDA and GGA functionals with lattice parameters at 10 and 300 K. Note that for better representation the y axis does not start at zero.

Besides from low-temperature specific-heat measurements, the density of states (DOS) close to the Fermi energy  $E_F$ , that determines the electronic and magnetic properties of metals, is accessible by measurements of the de Haas–van Alphen (dHvA) effect combined with electronic band-structure calculations. For layered systems, such as  $\text{SrCo}_2\text{P}_2$ , such calculations might particularly depend on calculational details because of the presence of electronic singularities connected to the low dimensionality of the compound. In the case of  $\text{SrCo}_2\text{P}_2$ , band-structure calculations applying the local density approximation (LDA) rather well compare with dHvA experiments [16]. The corresponding Co-dominated DOS shows a well-pronounced narrow peak in close vicinity to the Fermi level. In sharp contrast, such a peak is absent in another calculation, applying the general gradient approximation (GGA) in a different calculational setup (for details see technical section of Ref. [17]). Since the DOS and the underlying band structure near the Fermi level and the Co-related contribution is crucial for conclusions about the magnetic properties of a system, in particular, on the verge of ferromagnetism, a reinvestigation in this aspect seems desirable. However, in addition to the dependence on the exchange-correlation potential [18,19], for reliable results various parameters are required to be known precisely, such as the lattice parameters and internal positions of the atoms. This stimulated us to carry out low-temperature synchrotron

x-ray diffraction experiments to obtain reliable structural input parameters for our calculations.

In this paper, we conducted dHvA-effect measurements in high fields up to 35 T that reveal the FS topology of  $\text{SrCo}_2\text{P}_2$  in order to resolve the DOS close to  $E_F$  and its role concerning the occurrence of magnetic order. By comparing the experimental dHvA frequencies—including several previously not observed frequencies [16]—to those from band-structure calculations (using the experimentally determined low-temperature lattice parameters and different functionals), we identify the calculation that fits the data best. From that, we draw conclusions about the DOS at the Fermi energy that allow to discuss, for example, many-body interactions in  $\text{SrCo}_2\text{P}_2$ . As expected, the band structure is strongly influenced by the exact value of the Wyckoff position of P, that yields the distance  $z_p$  between Sr and P or  $d_{p,p}$  between P and P along [001], respectively. This value is temperature dependent which results in an implicit temperature dependence of the band structure that, in the present case, leads to an extraordinarily strong change in the DOS at  $E_F$ .

## II. METHODS

We prepared  $\text{SrCo}_2\text{P}_2$  single crystals in a tin flux with a residual resistivity ratio  $\rho(300\text{ K})/\rho(2\text{ K})$  of 80. We measured the dHvA effect of  $\text{SrCo}_2\text{P}_2$  by use of the capacitive torque method in fields up to 18 T and at temperatures down to 30 mK in a dilution refrigerator at the Dresden High Magnetic Field Laboratory (HLD). Although we obtained a wide spectrum of dHvA frequencies during these measurements, we did not observe any of the frequencies below 500 T that were predicted by band-structure calculations. Extending the field range gives the chance to detect these missing frequencies and at the same time allows for a higher dHvA-frequency resolution. Therefore, we conducted further dHvA experiments at higher fields up to 35 T at the Laboratoire National des Champs Magnétiques Intenses in Grenoble, France and in fields up to 33 T at the High Field Magnet Laboratory in Nijmegen, The Netherlands. We fixed the samples on CuBe cantilevers using vacuum grease. The torque magnetometer itself, mounted on a rotator, allowed us to determine the angular dependence of the dHvA oscillations. We rotated the sample relative to the applied magnetic field around the  $b$  axis (angle of rotation  $\theta_{010}$ ), around the  $ab$  axis ( $\theta_{110}$ ), and around the  $c$  axis ( $\theta_{001}$ ). We were able to detect quantum oscillations in the signal for all investigated directions.

The measurement of dHvA oscillations at different temperatures allows for the experimental determination of the effective masses according to the Lifshitz-Kosevich formula [20]. We performed these measurements in the dilution refrigerator at the HLD at different angles, and the obtained effective masses were compared to calculated band masses.

Besides the lattice parameters, a measure for the above-mentioned bond angle is the phosphorus position reflected in the distance  $z_p$  between Sr and P (see the structure in the inset of Fig. 1). Since the dHvA experiments are carried out at low temperatures, we performed powder x-ray diffraction at the beamline ID22 at the European Synchrotron Research Facility (ESRF) in Grenoble using a wavelength  $\lambda = 0.39997$  Å at

TABLE I. Lattice parameters of  $\text{SrCo}_2\text{P}_2$  at 10 K determined by using powder x-ray diffraction at the ESRF and at 300 K from Ref. [21].

	10 K	300 K
$c$ (Å)	11.6249	11.610
$a$ (Å)	3.7764	3.794
$c/a$	3.078	3.060
$z_p$ (Å)	4.100	4.092

10 K. This allowed us to obtain precise structural input for the DFT calculations.

We carried out electronic band-structure calculations for  $\text{SrCo}_2\text{P}_2$  using the full-potential local-orbital code (FPLO, version 15.02) [22,23]. We selected the local (spin) density approximation with the Perdew and Wang flavor [24] and the GGA with the Perdew-Burke-Ernzerhof flavor [25] of the exchange and correlation potentials. As lattice parameters, we applied the results listed in Table I [26]. To describe accurately potential singularities in the band structure (see Fig. 6 in Ref. [16]), we used a very fine  $60 \times 60 \times 60$  regular  $k$ -point mesh with resulting 146 71 points in the irreducible part of the Brillouin zone to obtain well-converged results with respect to the DOS and the band dispersion.

### III. RESULTS

#### A. Band-structure calculations

Figure 1(a) shows the total density of states (black line) and the partial contributions of the elements (colored lines) calculated by use of the GGA functional and the lattice parameters at 10 K. Independent of the details discussed in the following, our calculated DOS agrees well with Ref. [16] with respect to bandwidth, shape, and the contribution of the different elements, in particular, near the Fermi energy. Since both LDA and GGA functionals yield similar peaks at the Fermi level, we assign the disagreement with the calculations in Ref. [17] to the likely much too small  $k$ -point sampling therein. We note that also the width of the valence band therein is significantly different from Ref. [16] and our calculations. In Fig. 1(b), we show the DOS calculated using LDA in comparison with GGA for the lattice parameters determined at two temperatures (10 and 300 K). It is worth noting that the peaks in the DOS appear extremely close to the Fermi level, originating from almost dispersionless features in the band structure on the lines  $\Gamma$ - $X$  and  $Y_1$ - $Z$  (compare Fig. 5).

Depending on the used functional and lattice parameters this peak may lie directly at  $E_F$  or slightly above. This implies that the adequate choice of the functional and the structural parameters are crucial for an understanding of the appearance or absence of magnetism in the material. Indeed, the DOS at  $E_F$  is highly sensitive to the chosen parameters and varies by about a factor of almost 2. When changing the temperature from 300 to 10 K, the DOS at  $E_F$  reduces to about 69% of its room-temperature value (both calculations with the GGA functional).

We should mention that fully relativistic calculations including spin-orbit coupling do not change the band structure

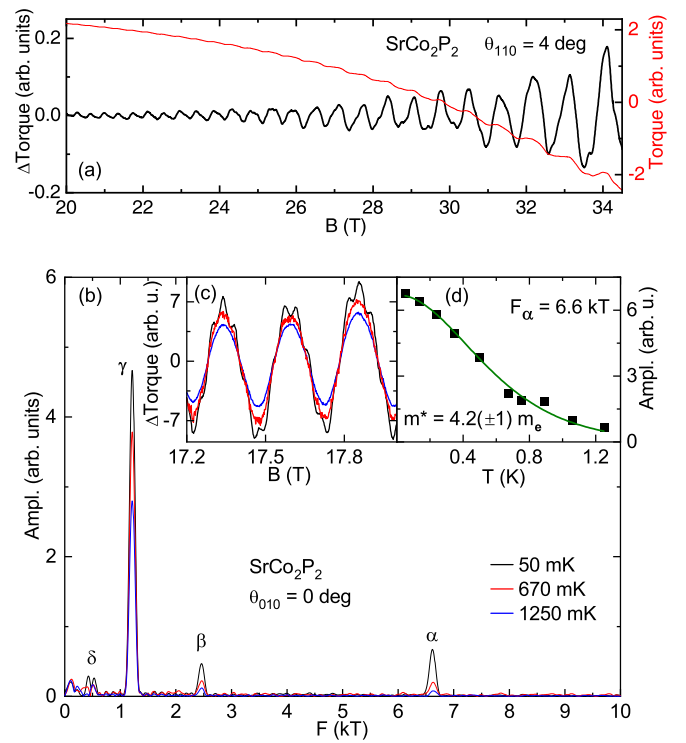


FIG. 2. (a) Torque signal as measured at  $\theta_{110} = 4^\circ$  up to 34.5 T (red line, right axis) and the oscillating part of the torque signal after background subtraction (black line, left axis). (b) dHvA frequency spectra for fields applied along the  $c$  direction after Fourier transformation of the background-subtracted torque signal between 14 and 18 T for selected temperatures. (c) Zoom on the torque signal around 17.6 T at 50 mK, 670 mK, and 1.25 K. (d) Amplitude of the  $\alpha$  frequency between 50 mK and 1.25 K (black squares) and the corresponding fit using the Lifshitz-Kosevich formula [20].

close to  $E_F$ . In order to decide which of the calculations fits best with reality a comparison with experimental data is needed. For that, we performed comprehensive dHvA studies.

#### B. Torque magnetometry

Figure 2(a) shows typical as-measured (red line) and background-subtracted data (black line) of the torque signal up to 34.5 T at  $\theta_{110} = 4^\circ$ . The background changes considerably reflecting the strong paramagnetism in  $\text{SrCo}_2\text{P}_2$ . Nevertheless, we can resolve clear dHvA oscillations even on the as-measured data that become more prominent after background subtraction. Figure 2(b) shows the spectral distribution of the dHvA frequencies at  $\theta_{010} = 0^\circ$  (field along the  $c$  direction). We obtained the spectrum with four main peaks by fast Fourier transformation of the oscillating part of the measured signal presented in Fig. 2(c) for a narrow field range around 17.6 T. We show the effect of temperature on the dHvA signal for three different temperatures in Figs. 2(b) and 2(c). We can nicely describe the temperature-dependent dHvA amplitude by using the Lifshitz-Kosevich formula [20] as shown in Fig. 2(d) for the amplitude of frequency  $\alpha$ . From this fit, we obtain an effective mass of  $m^* = 4.2m_e$  with  $m_e$  as the free-electron mass.

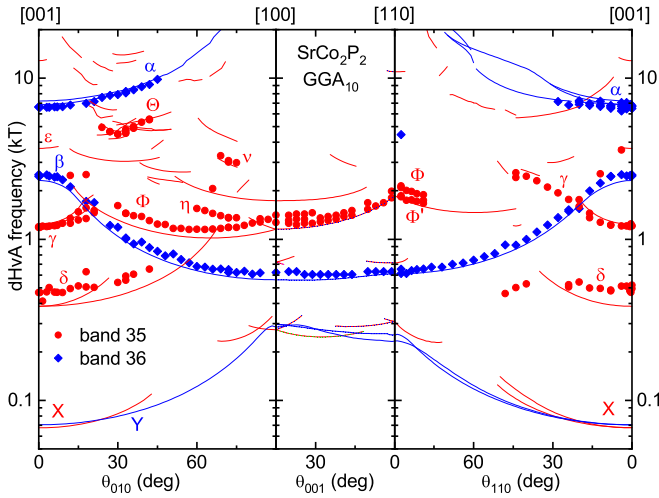


FIG. 3. Angular dependence of the experimentally observed dHvA frequencies (symbols) and of the calculated extremal Fermi-surface cross sections (lines) in  $\text{SrCo}_2\text{P}_2$ . For the calculations, we used the GGA functional and lattice parameters determined at 10 K (GGA<sub>10</sub>). The line colors correspond to the FS colors shown in Fig. 5(b).

In Fig. 3, we show the angular dependence of the experimentally determined dHvA frequencies (symbols) together with the calculated frequencies using the GGA functional and structural parameters at 10 K (lines). We observe several dHvA branches with frequencies between 0.4 and 10 kT labeled with Greek letters. These branches are caused by extremal orbits on Fermi surfaces from two bands crossing the Fermi energy. The color coding of the experimental data is according to these two bands and will be discussed in the following paragraph. We state a very good correspondence between our experimental data and those published in Ref. [16] apart from smaller deviations and our ability to observe dHvA oscillations of the branch  $\delta$ , not seen in Ref. [16]. We did not observe low dHvA frequencies of less than 400 T, such as those of the frequency branches X and Y, probably due to the strong magnetic background in the torque signal [see Fig. 2(a)]. This background is fit by a polynomial, which then is subtracted from the raw data. For a strong background a high-order polynomial is needed, which may lead to a subtraction of slow oscillations with weak amplitude from the signal.

### C. Sensitivity to functionals and structural parameters

As mentioned, the adequate choice of the functional as well as the structural parameters is essential for a proper theoretical description of the band structure. Figure 4 shows the experimental data compared to band-structure calculations using the GGA functional performed with the structural parameters at 300 and 10 K given in Table I. We achieve a better correspondence with using the data derived from the low-temperature structure, especially concerning the size of the  $\beta$  orbit (see also Fig. 3). For the 300-K data a third band (band 37) crosses the Fermi energy and leads to small pockets with frequencies that lie between 100 and 1000 T and that have not been observed experimentally.

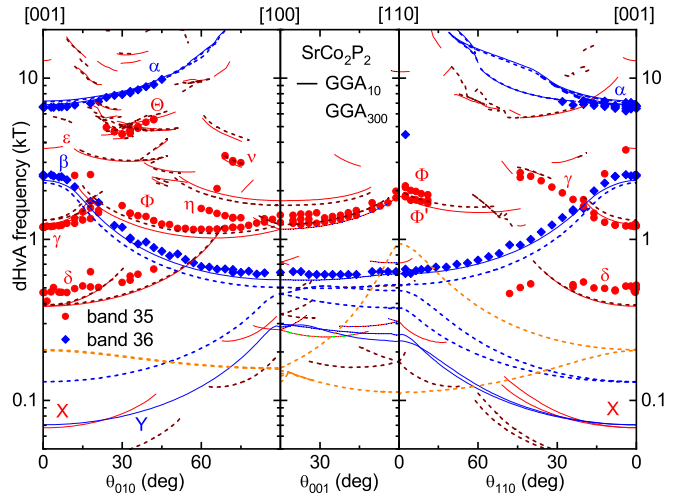


FIG. 4. Comparison between results of the calculation using the GGA functional with structural parameters at 300 K (dashed lines) and at 10 K (solid lines) together with the angular-dependent experimental data shown already in Fig. 3. The (dark) red line colors correspond to calculated extremal areas of band 35, blue for band 36, and orange for band 37. The latter does not appear for the GGA with 10-K parameters.

When using the GGA functional and the 10-K lattice parameters, there are two bands crossing the Fermi energy, shown in Fig. 5(a). We show the corresponding FS sheets in Fig. 5(b). Band 35 leads to a rather complicated FS structure (red) of four strongly warped cylinders in the first Brillouin zone (BZ), which are cut through by holes perpendicular to the cylinder axes. This FS has a holelike character. The second FS sheet (blue) results from band 36 and consists of a deformed cylinder that is distributed over the corners of the BZ, of a closed pillow around Z, and a small ellipsoid at roughly half the way from the center to the BZ corner. The FS from band 36 is electronlike.

By comparing the experimental data to the calculated frequencies and FSs, we can assign the different extremal orbits to the measured frequency branches. Frequency  $\alpha$  clearly follows a  $1/\cos(\theta)$  behavior corresponding to the cylindrically shaped FS sheet (band 36) in Fig. 5(b). We can assign the smaller pillow from the same band to frequency  $\beta$ . All other observed frequencies ( $\gamma$ ,  $\delta$ ,  $\Theta$ ,  $\nu$ ,  $\eta$ ,  $\Phi$ ) originate from the multiply connected FS of band 35.

In order to investigate the influence of the functional, we performed FPLO calculations using the low-temperature (10-K) structural parameters and a different functional LDA. Figure 5(a) shows the dispersion of the energy bands close to the Fermi energy calculated for the GGA and LDA functionals with 10-K structural parameters. For the LDA functional, too, a third band crosses the Fermi energy (band 37, plotted in orange) and leads to a small FS sheet in the corners of the BZ (not shown). The frequencies that correspond to the extremal areas of this FS are absent in the dHvA experiment as the comparison in Fig. 6 shows. Especially for fields aligned along [110], the calculations predict dHvA frequencies up to about 1000 T that should easily be observable.

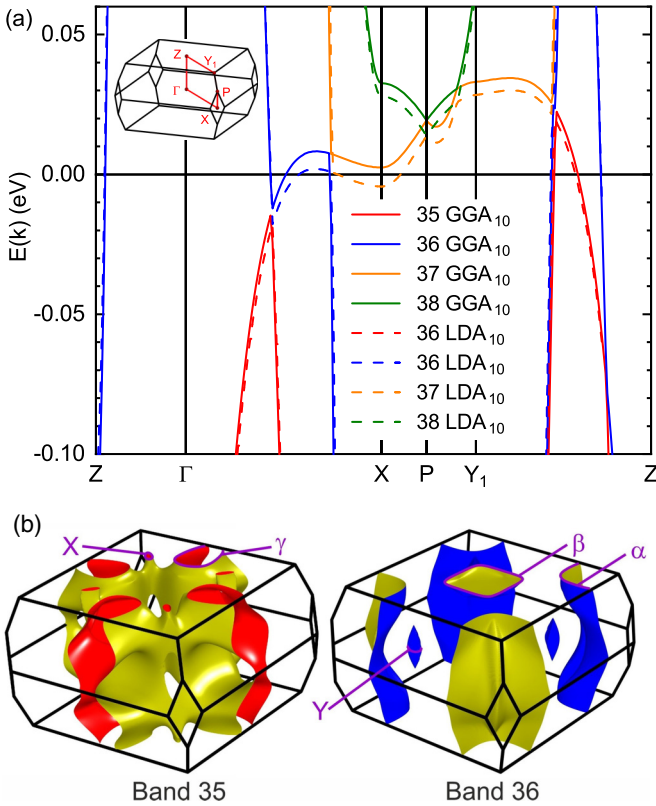


FIG. 5. (a) Band dispersion of  $\text{SrCo}_2\text{P}_2$  near the Fermi energy calculated using two different potentials: GGA (full lines,  $\text{GGA}_{10}$ ) and LDA (dashed lines,  $\text{LDA}_{10}$ ) both with using the 10-K lattice parameters. In the former case, two bands, 35 (red) and 36 (blue) cross  $E_F$  for the latter case, three bands, 35 (red), 36 (blue), and 37 (orange) cross  $E_F$ . (b) Calculated Fermi surfaces for bands 35 (red) and 36 (blue) using  $\text{GGA}_{10}$ .

Following the temperature dependence of the dHvA oscillation amplitudes, we determined the effective masses of the quasiparticles on experimentally observed orbits as described above and shown, for one example, in Fig. 2(d). Table II lists the experimentally determined effective masses with corresponding dHvA frequencies as well as calculated masses (using GGA functionals with 10-K structural parameters) and the corresponding mass-enhancement factors for different angles. The cylinder (orbit  $\alpha$ ) of band 36 shows effective masses between four and six free-electron masses, the pillow (orbit  $\beta$ ) shows masses between 0.8 and  $2.7m_e$ , and the masses of the quasiparticles of band 35 lie between 0.8 and  $4.2m_e$ . The mass-enhancement factor is about 2 on average.

#### IV. DISCUSSION

We obtain the best correspondence between experiment and theory for the calculation using the GGA functional in combination with the experimental structural data at 10 K. A deviation in the size of the FSs from the experimental results appears when either using GGA with the 300 K or LDA with 10-K lattice parameters. But, more importantly, for all other calculations apart from GGA with 10-K parameters, a third band crosses the Fermi energy leading to a FS that has not been observed experimentally. In consequence, this means

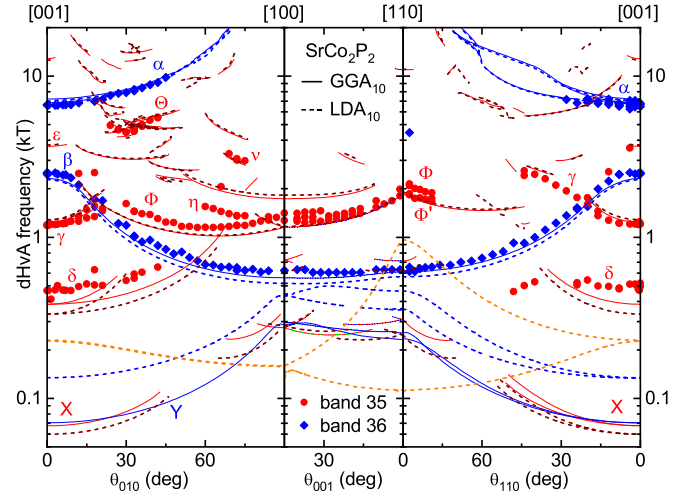


FIG. 6. Comparison between results of the calculation with GGA (solid lines) and LDA (dashed lines) functionals for structural parameters obtained at 10 K.

that the DOS at  $E_F$  at 10 K is significantly reduced compared to the room-temperature structure. The Co  $3d$ -related partial DOS is reduced to a value of about 1.3 states per eV, Co atom, and spin. This reduced value is only moderately above a simple estimate for ferromagnetic ordering in a Stoner-like picture where a  $3d$  DOS of about 1 state per eV, Co atom, and spin should induce band ferromagnetism. The absence of band ferromagnetism in the material might be related to

TABLE II. Experimentally determined dHvA frequencies ( $F_{\text{exp}}$ ) and effective masses ( $m^*$ ) of  $\text{SrCo}_2\text{P}_2$  for different angles together with the calculated frequencies ( $F_{\text{calc}}$ ) and bare band-structure masses ( $m_b$ ) with corresponding mass-enhancement factors ( $m^*/m_b$ ) using the GGA functional and lattice parameters at 10 K. The naming of the orbits is according to Fig. 3.

Orbit	Experiment		Calculations		
	$F_{\text{exp}}$ (kT)	$m^*$ ( $m_e$ )	$F_{\text{calc}}$ (kT)	$m_b$ ( $m_e$ )	$m^*/m_b$
$B \parallel [001] (\theta_{010} = \theta_{110} = 0^\circ)$					
$\alpha$	6.615	4.2(1)	6.838	2.26	1.9
$\beta$	2.457	2.7(2)	2.317	1.14	2.4
$\gamma$	1.197	1.58(3)	1.239	0.8	2.0
$\delta$	0.468		0.384		
$\theta_{010} = 33^\circ$					
$\alpha$	8.258	6.1(2)	8.252	3.43	1.8
$\beta$	1.004	1.2(1)	0.957	0.65	1.9
$\delta$	0.558	4.1(4)	0.462	1.13	3.6
$\Theta$	4.799	4.2(7)	4.800	2.9	1.5
$\Phi$	1.451	0.94(11)	1.257	0.57	1.6
$\theta_{010} = 72^\circ$					
$\beta$	0.648	0.83(5)	0.586	0.42	2.0
$\gamma$	3.024	1.9(1)	2.980	1.11	1.7
$\eta$	1.368	1.30(6)			
$\Phi$	1.188	0.84(3)	1.028	0.44	1.9
$\theta_{110} = 86^\circ$					
$\beta$	0.632	1.1(1)	0.612	0.37	3.0
$\Phi$	1.853	1.7(4)	1.737	0.97	1.8

the quasi-two-dimensional elements in its electronic structure, competing different magnetic ordering vectors or simply to the incomplete description of many-body effects in the framework of DFT.

Although the FS of SrCo<sub>2</sub>P<sub>2</sub> has pronounced two-dimensional elements, namely, the cylinders of band 36, it also displays three-dimensional features, such as the pillow and small ellipsoid of band 36 and the rather evolved FS topology of band 35 with the holes perpendicular to [001]. This is rather unusual for a system with such a long distance  $d_{p,p}$  of 3.425 Å. SrFe<sub>2</sub>P<sub>2</sub>, for example, has the same structure and a comparable distance between the transition metal and the phosphorus atom along [001] (3.434 Å) but possesses a much more pronounced two-dimensional FS with corrugated cylinders, sometimes, however, with strong warping [6]. In neither of the two compounds FS nesting or hints towards a magnetic instability has been observed. Consequently, superconductivity with  $s\pm$  pairing is not to be expected either.

For nearly ferromagnetic materials, it has been reported that some dHvA frequencies show a field-dependent splitting [27–29]. Although we observe the two close-by frequencies  $\Phi$  and  $\Phi'$ , that can be seen in Fig. 3(a) for  $\theta_{001}$  and  $90^\circ \geq \theta_{110} \geq 75^\circ$ , this splitting is neither field nor temperature dependent. The origin of these double peaks is unclear but could be due to a slight misalignment of layers that are stapled along the [001] direction.

We find effective masses between about one and four free-electron masses when the magnetic field is applied parallel to the  $c$  axis (Table II). Compared to the calculated masses, the experimental masses are larger by roughly a factor of 2. This compares well to the mass enhancement estimated from the measured and calculated Sommerfeld coefficient  $\gamma$  of the electronic part of the specific heat. Using the value of 6.9 states/(eV f.u.) for the DOS at  $E_F$  (GGA functional, 10 K, see Fig. 1), results in  $\gamma_{\text{calc}} \approx 16 \text{ mJ mol}^{-1} \text{ K}^{-2}$ . Combined with the experimental value of  $\gamma \approx 40 \text{ mJ mol}^{-1} \text{ K}^{-2}$  [8,16],

we estimate a mass enhancement of 2.5, averaged over all bands and orientations. This evidences an appreciable renormalization due to many-body interactions and may indicate the closeness to a magnetic ground state.

## V. CONCLUSIONS

Our detailed FS study of SrCo<sub>2</sub>P<sub>2</sub> by use of density-functional-theory band-structure calculations showed an extreme sensitivity of the DOS at  $E_F$  on structural parameters and the chosen functionals. Our dHvA results are in excellent agreement with calculations using the GGA functional and 10-K lattice parameters. This reveals a strongly reduced rather modest DOS at  $E_F$  which suggests why SrCo<sub>2</sub>P<sub>2</sub> does not order ferromagnetically.

The knowledge on the high sensitivity of the band structure on subtle lattice-parameter changes allows, in principle, for a directed modification of the electronic properties. An increase in the DOS at  $E_F$  and, consequently, inducing ferromagnetism should be possible by decreasing the  $c/a$  ratio, i.e., by the application of a moderate uniaxial strain decreasing the  $c$  axis (see Table I).

## ACKNOWLEDGMENTS

We acknowledge support from the Deutsche Forschungsgemeinschaft (DFG) through GRK 1621 and the Würzburg-Dresden Cluster of Excellence on Complexity and Topology in Quantum Matter–*ct.qmat* (EXC 2147, Project No. 390858490), the ANR-DFG Grant "Fermi-NESt," by the European Research Council (ERC) under the European Union's Horizon 2020 Research and Innovation Program (Grant Agreement No. 681260) as well as the support of the HLD at HZDR, the LNCMI-CNRS, and the HFML, members of the European Magnetic Field Laboratory (EMFL). U. Nitzsche (IFW Dresden) is acknowledged for technical support.

- 
- [1] J. Custers, P. Gegenwart, H. Wilhelm, K. Neumaier, Y. Tokiwa, O. Trovarelli, C. Geibel, F. Steglich, C. Pepin, and P. Coleman, *Nature (London)* **424**, 524 (2003).
  - [2] F. Steglich, J. Aarts, C. D. Bredl, W. Lieke, D. Meschede, W. Franz, and H. Schäfer, *Phys. Rev. Lett.* **43**, 1892 (1979).
  - [3] R. Hoffmann and C. Zheng, *J. Phys. Chem.* **89**, 4175 (1985).
  - [4] S. Jia, P. Jiramongkolchai, M. R. Suchomel, B. H. Toby, J. G. Checkelsky, N. P. Ong, and R. J. Cava, *Nat. Phys.* **7**, 207 (2011).
  - [5] A. I. Coldea, C. M. J. Andrew, J. G. Analytis, R. D. McDonald, A. F. Bangura, J.-H. Chu, I. R. Fisher, and A. Carrington, *Phys. Rev. Lett.* **103**, 026404 (2009).
  - [6] J. G. Analytis, C. M. J. Andrew, A. I. Coldea, A. McCollam, J.-H. Chu, R. D. McDonald, I. R. Fisher, and A. Carrington, *Phys. Rev. Lett.* **103**, 076401 (2009).
  - [7] F. Ronning, E. D. Bauer, T. Park, S.-H. Baek, H. Sakai, and J. D. Thompson, *Phys. Rev. B* **79**, 134507 (2009).
  - [8] S. Jia, A. J. Williams, P. W. Stephens, and R. J. Cava, *Phys. Rev. B* **80**, 165107 (2009).
  - [9] M. S. Torikachvili, S. L. Bud'ko, N. Ni, and P. C. Canfield, *Phys. Rev. Lett.* **101**, 057006 (2008).
  - [10] A. Kreyssig, M. A. Green, Y. Lee, G. D. Samolyuk, P. Zajdel, J. W. Lynn, S. L. Bud'ko, M. S. Torikachvili, N. Ni, S. Nandi, J. B. Leão, S. J. Poulton, D. N. Argyriou, B. N. Harmon, R. J. McQueeney, P. C. Canfield, and A. I. Goldman, *Phys. Rev. B* **78**, 184517 (2008).
  - [11] S. Jia, S. Chi, J. W. Lynn, and R. J. Cava, *Phys. Rev. B* **81**, 214446 (2010).
  - [12] H.-H. Wen and S. Li, *Annu. Rev. Condens. Matter Phys.* **2**, 121 (2011).
  - [13] K. Kuroki, H. Usui, S. Onari, R. Arita, and H. Aoki, *Phys. Rev. B* **79**, 224511 (2009).
  - [14] C.-H. Lee, A. Iyo, H. Eisaki, H. Kito, M. T. Fernandez-Diaz, T. Ito, K. Kihou, H. Matsuhata, M. Braden, and K. Yamada, *J. Phys. Soc. Jpn.* **77**, 083704 (2008).
  - [15] S. Jia and R. J. Cava, *Phys. Rev. B* **82**, 180410(R) (2010).
  - [16] A. Teruya, A. Nakamura, T. Takeuchi, H. Harima, K. Uchima, M. Hedo, T. Nakama, and Y. Onuki, *J. Phys. Soc. Jpn.* **83**, 113702 (2014).
  - [17] E. Cuervo-Reyes and R. Nesper, *Phys. Rev. B* **90**, 064416 (2014).

- [18] S. Blackburn, B. Prévost, M. Bartkowiak, O. Ignatchik, A. Polyakov, T. Förster, M. Côté, G. Seyfarth, C. Capan, Z. Fisk, R. G. Goodrich, I. Sheikin, H. Rosner, A. D. Bianchi, and J. Wosnitza, *Phys. Rev. B* **89**, 220505(R) (2014).
- [19] T. Förster, I. Kraft, I. Sheikin, A. D. Bianchi, J. Wosnitza, and H. Rosner, *J. Phys.: Condens. Matter* **32**, 025503 (2020).
- [20] D. Shoenberg, *Magnetic Oscillations in Metals* (Cambridge University Press, London, 1984).
- [21] A. Mewis, *Z. Naturforsch., B: J. Chem. Sci.* **35**, 141 (1980).
- [22] K. Koepnik, B. Velický, R. Hayn, and H. Eschrig, *Phys. Rev. B* **55**, 5717 (1997).
- [23] K. Koepnik and H. Eschrig, *Phys. Rev. B* **59**, 1743 (1999).
- [24] J. P. Perdew and Y. Wang, *Phys. Rev. B* **45**, 13244 (1992).
- [25] J. P. Perdew, K. Burke, and M. Ernzerhof, *Phys. Rev. Lett.* **77**, 3865 (1996).
- [26] The LDA and GGA functionals are the most commonly used approximations which allow for a quite accurate calculation of physical properties. Although LDA only calculates the electron density at a point in  $k$  space, GGA also takes the gradient of the electron density into account in order to correct for an inhomogeneous electron density.
- [27] G. G. Lonzarich, *J. Magn. Magn. Mater.* **45**, 43 (1984).
- [28] S. M. Hayden, G. G. Lonzarich, and H. L. Skriver, *J. Magn. Magn. Mater.* **54-57**, 1013 (1986).
- [29] J. M. van Ruitenbeek, A. P. J. van Deursen, L. W. M. Schreurs, R. A. de Groot, A. R. de Vroomen, Z. Fisk, and J. Smith, *J. Phys. F: Met. Phys.* **14**, 2555 (1984).